

Binary Stellar Population Synthesis Study of Elliptical Galaxies

Zhongmu Li^{1,2}*, Fenghui Zhang¹ and Zhanwen Han¹

¹ National Astronomical Observatories/Yunnan Observatory, the Chinese Academy of Sciences, Kunming, 650011, China

² Graduate School of the Chinese Academy of Sciences

Received 2001 month day; accepted 2001 month day

Abstract We determine relative stellar ages and metallicities mainly for about 80 elliptical galaxies in low and high density environments via the latest binary stellar population (BSP) synthesis model and test a latest hierarchical formation model of elliptical galaxies which adopted the new Λ CDM cosmology for the first time. The stellar ages and metallicities of galaxies are estimated from two high-quality published spectra line indices, i.e. H β and [MgFe]. The results show that elliptical galaxies have stellar populations older than 3.9 Gyr and more metal rich than 0.02. Most of our results are in agreement with predictions of the model: First, elliptical galaxies in denser environment are redder and have older populations than field galaxies. Second, elliptical galaxies with more massive stellar components are redder while have older and more metal rich populations than less massive ones. Third, the most massive galaxies are shown to have the oldest and most metal rich stars. However, some of our results are found to be different with predictions of the galaxy formation model, i.e. the metallicity distributions of low- and high-density elliptical galaxies and the relations relating to cluster-centric distance.

Key words: galaxies: stellar content — galaxies: formation — galaxies: elliptical and lenticular, cD

1 INTRODUCTION

Now it is a golden era to study galaxy formation and evolution. Fortunately, elliptical galaxies supply us a good chance to carry out this work because they seem to be homogeneous stellar systems that have uniformly old and red populations. Besides, elliptical galaxies have negligible amounts of gas and have very little star formation. Therefore, it is convenient to study galaxy formation via ellipticals first. After the significant development of cosmology (e.g. Peebles 1980), the image that galaxies formed in a universe dominated by dark matter was widely accepted.

* E-mail: zhongmu.li@gmail.com

But people are still arguing about the mechanism of elliptical galaxy formation. Recently, there are mainly two arguing pictures of elliptical galaxies' formation. On the one hand, some people suggest that elliptical galaxies formed in a single intense burst of star formation at high redshifts and then their stellar populations passively evolved to the present day. This "monolithic" scenario can explain the dense cores, metallicity gradients (Kormendy 1987; Thomsen & Baum 1989; Kormendy & Djorgovski 1989) and fundamental scaling relations such as the colour-magnitude relation and the fundamental plane of elliptical galaxies (Kodama et al. 1998; van Dokkum & Stanford 2003), but it cannot explain different metallicity levels of halo stars and the big age range of globular clusters. On the other hand, based on evidence of strong gravitational interactions and mergers between disk galaxies, Toomre & Toomre et al. (1972) pointed out that elliptical galaxies are possibly formed by the merging of smaller galaxies. It is very the so-called "hierarchical" scenario of galaxy formation.

In recent years, the hierarchical picture is thought as the most possible mechanism of galaxies and was deeply simulated, e.g. Kauffmann et al. (1993, 1996, 1998) and Durham group (Baugh et al. 1996, Baugh et al. 1998, Cole et al. 2000). In these studies, some exciting results are presented, e.g. the star formation histories of galaxies (see e.g. Baugh et al. 1998). But on the observational side, studies showed some different trends: Firstly, it is found that a significant fraction of early-type galaxies have recent star formation (Barger et al. 1996). Secondly, it is also found that only a small fraction of mass is involved in the interaction and merger of galaxies. And thirdly, some related issues, e.g. the super-solar $[\alpha/\text{Fe}]$ ratio of massive ellipticals, which suggests these galaxies formed on relatively short time-scales and have an initial mass function that is skewed towards massive stars, have brought forward. It seems that those early models of the hierarchical formation of elliptical galaxies are difficult to explain and reproduce these observed trends (Thomas 1999). In 2006, De Lucia et al. (2006) brought forward a new hierarchical model of the formation of elliptical galaxies. This model, adopting the new ΛCDM cosmology and high-resolution simulation, tried to explain the "anti-hierarchical" behavior of star formation histories of elliptical galaxy population and presented some new predictions. Therefore, it is more valuable to study the formation of elliptical galaxies based on this kind new models now.

To study galaxy formation, stellar population synthesis has become a very useful and popular technique in these years because different galaxy formation models usually predict different star formation histories. A series of detailed studies of stellar populations of galaxies in both observational side and semi-analytic side have been carried out in recent years (e.g. Trager et al. 2000a, b; Terlevich & A. Forbes D. 2002; van Zee et al. 2004). However, all these works used the single stellar population (SSP) synthesis models (e.g. Vazdekis et al. 1996, 1997; Vazdekis 1999; Worthey 1994; Bruzual & Charlot et al. 2003) as the binary stellar population (BSP) synthesis model was not available. But as pointed out by Zhang et al. (2005a, b), binary interaction plays an important role in the study of evolutionary population synthesis. In their work, some different results from SSP models were shown (see Zhang 2005a in more detail). Thus we are now asking the question that how hierarchical formation model of elliptical galaxies is supported if we take the binary interaction in stellar population synthesis into account. We plan to find some answers by making use of the BSP model of Zhang et al. (2005b) and the hierarchical formation model of De Lucia et al. (2006) in this paper. But we here do not intend to investigate the effects of binary interaction, which is very the subject of another paper. The structure of the paper is as follows. In Sect. 2 we introduce our galaxy sample and the BSP model. In Sect. 3 we give a brief description of the determination of stellar ages and metallicities and then show the main results. In Sect. 4 we test the latest hierarchical formation model of elliptical galaxies and finally we give our discussion and conclusion in Sect. 5.

2 OUR DATA SAMPLE AND THE BSP MODEL

2.1 The galaxy sample

We mainly define a sample by selecting all normal elliptical galaxies in the sample of Thomas et al. (2005). As a result, 71 normal elliptical galaxies are included while 51 S0 and 2 cD galaxies are excluded by our sample. Then the $B - V$ colors and B-band absolute magnitudes of these galaxies are supplemented from the HyperLeda database (<http://www.brera.mi.astro.it/hypercat/>) if it is possible. In the sample, 42 elliptical galaxies reside in low-density and 29 in high-density environments. The galaxies in low-density environment include all galaxies that do not reside in high-density environment. In fact, these data are very good for estimating stellar ages and metallicities because they were selected from some creditable sources (González 1993; Mehlert et al. 2000, 2003; Beuing et al. 2002; Lauberts & Valentijn 1989) and reobserved by Thomas et al. if necessary (19 objects were reobserved). In particular, because the absorption-line strengths of galaxies are measured as functions of galaxy radius in the sources, the central indices measured within $r_e/10$ (where r_e is the effective radius) are adopted, so that the analysis does not suffer from aperture effects. In this work, we use the reliable Lick indices $H\beta$, Mgb , and $\langle Fe \rangle = 0.5 \times (Fe5270 + Fe5335)$ directly. According to Thomas et al., the medians of the 1σ errors in $H\beta$, Mgb , $Fe5270$ and $Fe5335$ are 0.06, 0.06, 0.07 and 0.08, respectively. It is also another advantage to take these data because these elliptical galaxies span a large range in central velocity dispersion $0 \leq \sigma_0/(\text{km s}^{-1}) \leq 340$, which is very convenient to study the relations between stellar specialities and stellar mass following the result of Thomas et al. (2005). The detailed data of our sample galaxies are shown in Table 1. In the table, the galaxy name, velocity dispersion, $H\beta$, Mgb , $\langle Fe \rangle$, M_B , $B - V$, environment and the observational uncertainties of three line indices are shown. Besides, we also select 11 elliptical galaxies in the Fornax cluster from Kuntschner (2000), but they are only used for testing the predictions relating to cluster-centric distance.

2.2 The BSP model

In this work, we translate central line indices of galaxies into stellar ages and metallicities via the BSP model of Zhang et al. (2005b). This model supplied us with high-resolution (0.3 Å) absorption-lines defined by the Lick Observatory Image Dissector Scanner (Lick/IDS) system for an extensive set of instantaneous burst binary stellar populations with binary interactions. In particular, its stellar populations span an age range 1–15 Gyr and a metallicity range 0.004–0.03.

3 STELLAR AGES AND METALLICITIES OF ELLIPTICAL GALAXIES

To determine BSP-equivalent stellar ages and metallicities of elliptical galaxies, we use $H\beta$ and $[MgFe]$ (González 1993) indices in this work. The latter can be calculated by $\sqrt{Mgb} \times 0.5 \times (Fe5270 + Fe5335)$. Fig. 1 displays the $H\beta$ and $[MgFe]$ indices of the 71 elliptical galaxies overlaid onto the theoretical calibration. The open and filled circles represent ellipticals in low- and high-density environments respectively and the error bars show the observational uncertainties of two indices.

The BSP-equivalent stellar age, metallicity of each elliptical galaxy is determined by choosing the best-fitting (t, Z) in a grid of stellar age (t) and metallicity (Z). The grid is elaborate enough and created by interpolating the BSP models at intervals $\Delta t = 0.1$ Gyr and $\Delta Z = 0.0001$. To find the best-fitting (t, Z) , we employ the maximum-likelihood fitting method. In

Table 1 The data for low- and high-density ellipticals. In the table, ‘ σ_0 ’ means the velocity dispersion and ‘E’ means the environment. ‘L’ and ‘H’ denotes low- and high-density environments, respectively. All line indices are within $r_e/10$ aperture.

Name	σ_0 [km s ⁻¹]	H β [Å]	$\delta H\beta$ [Å]	Mgb [Å]	δMgb [Å]	$\langle Fe \rangle$ [Å]	$\delta \langle Fe \rangle$ [Å]	M_B [mag]	$B - V$ [mag]	E
NGC 0221	72.1	2.31	0.05	2.96	0.03	2.75	0.03	-17.424	0.800	L
NGC 0315	321.0	1.74	0.06	4.84	0.05	2.88	0.05	-22.472	0.929	L
NGC 0507	262.2	1.73	0.09	4.52	0.11	2.78	0.10	-22.121	0.888	L
NGC 0547	235.6	1.58	0.07	5.02	0.05	2.82	0.05	-21.663		L
NGC 0636	160.3	1.89	0.04	4.20	0.04	3.03	0.04	-19.798	0.908	L
NGC 0720	238.6	1.77	0.12	5.17	0.11	2.87	0.09	-20.786	0.948	L
NGC 0821	188.7	1.66	0.04	4.53	0.04	2.95	0.04	-20.753	0.865	L
NGC 1453	286.5	1.60	0.06	4.95	0.05	2.98	0.05	-21.613	0.911	L
NGC 1600	314.8	1.55	0.07	5.13	0.06	3.06	0.06	-22.419	0.923	L
NGC 1700	227.3	2.11	0.05	4.15	0.04	3.00	0.04	-21.903	0.890	L
NGC 2300	251.8	1.68	0.06	4.98	0.05	2.97	0.05	-20.754	0.966	L
NGC 2778	154.4	1.77	0.08	4.70	0.06	2.85	0.05	-19.206	0.889	L
NGC 3377	107.6	2.09	0.05	3.99	0.03	2.61	0.03	-19.169	0.820	L
NGC 3379	203.2	1.62	0.05	4.78	0.03	2.86	0.03	-20.608	0.927	L
NGC 3608	177.7	1.69	0.06	4.61	0.04	2.94	0.04	-19.733	0.909	L
NGC 3818	173.2	1.71	0.08	4.88	0.07	2.97	0.06	-19.400	0.908	L
NGC 4278	232.5	1.56	0.05	4.92	0.04	2.68	0.04	-19.359	0.895	L
NGC 5638	154.2	1.65	0.04	4.64	0.04	2.84	0.04	-19.974	0.892	L
NGC 5812	200.3	1.70	0.04	4.81	0.04	3.06	0.04	-20.450	0.927	L
NGC 5813	204.8	1.42	0.07	4.65	0.05	2.67	0.05	-21.113	0.916	L
NGC 5831	160.5	2.00	0.05	4.38	0.04	3.05	0.03	-19.813	0.897	L
NGC 6127	238.9	1.50	0.05	4.96	0.06	2.85	0.05	-21.352	0.944	L
NGC 6702	173.8	2.46	0.06	3.80	0.04	3.00	0.04	-21.613	0.839	L
NGC 7052	273.8	1.48	0.07	5.02	0.06	2.84	0.05	-21.199		L
NGC 7454	106.5	2.15	0.06	3.27	0.05	2.48	0.04	-19.930	0.866	L
NGC 7785	239.6	1.63	0.06	4.60	0.04	2.91	0.04	-21.375	0.949	L
ESO 107-04	147.0	2.24	0.25	3.63	0.16	2.97	0.09	-20.386	0.849	L
ESO 148-17	134.5	2.26	0.52	3.49	0.32	2.58	0.20	-19.865	0.875	L
IC 4797	220.6	1.92	0.26	4.52	0.18	2.75	0.10	-20.876	0.908	L
NGC 0312	254.8	1.83	0.09	4.56	0.08	2.48	0.05	-21.937	0.929	L
NGC 0596	161.8	2.12	0.05	3.95	0.04	2.81	0.03	-20.424	0.845	L
NGC 0636	178.5	1.86	0.26	4.38	0.17	2.83	0.09	-19.798	0.908	L
NGC 1052	202.6	1.22	0.04	5.53	0.03	2.77	0.02	-20.139	0.900	L
NGC 1395	250.0	1.62	0.05	5.21	0.04	2.93	0.03	-21.211	0.921	L
NGC 1407	259.7	1.67	0.07	4.88	0.06	2.85	0.03	-21.432	0.946	L
NGC 1549	203.3	1.79	0.03	4.39	0.03	2.88	0.02	-19.981	0.906	L
NGC 2434	180.4	1.87	0.13	3.72	0.10	2.87	0.07	-19.828	0.818	L
NGC 2986	282.2	1.48	0.06	4.97	0.05	2.92	0.03	-21.064	0.891	L
NGC 3078	268.1	1.12	0.09	5.20	0.07	3.16	0.04	-20.893	0.916	L
NGC 3923	267.9	1.87	0.08	5.12	0.07	3.07	0.04	-21.151	0.906	L
NGC 5791	271.8	1.60	0.19	5.06	0.15	3.30	0.10	-21.123	0.89	L
NGC 5903	209.2	1.68	0.10	4.44	0.08	2.90	0.05	-21.220	0.839	L
NGC 4261	288.3	1.34	0.06	5.11	0.04	3.01	0.04	-21.299	0.952	H
NGC 4374	282.1	1.51	0.04	4.78	0.03	2.82	0.03	-20.888	0.931	H
NGC 4472	279.2	1.62	0.06	4.85	0.06	2.91	0.05	-21.785	0.928	H
NGC 4478	127.7	1.84	0.06	4.33	0.06	2.94	0.05	-19.564	0.873	H

Table 1 – Continued

Name	σ_0 [km s ⁻¹]	H β [Å]	$\delta H\beta$ [Å]	Mgb [Å]	δMgb [Å]	$\langle Fe \rangle$ [Å]	$\delta \langle Fe \rangle$ [Å]	M_B [mag]	$B - V$ [mag]	E
NGC 4489	47.2	2.39	0.07	3.21	0.06	2.66	0.05	-18.189	0.804	H
NGC 4552	251.8	1.47	0.05	5.15	0.03	2.99	0.03	-20.798	0.936	H
NGC 4697	162.4	1.75	0.07	4.08	0.05	2.77	0.04	-21.239	0.869	H
NGC 7562	248.0	1.69	0.05	4.54	0.04	2.87	0.04	-21.416	0.938	H
NGC 7619	300.3	1.36	0.04	5.06	0.04	3.06	0.04	-21.973	0.925	H
NGC 7626	253.1	1.46	0.05	5.05	0.04	2.83	0.04	-21.673	0.947	H
NGC 4839	275.5	1.42	0.04	4.92	0.04	2.75	0.04	-22.263	0.879	H
NGC 4841A	263.9	1.53	0.05	4.51	0.05	2.89	0.04	-21.380		H
NGC 4926	273.3	1.50	0.06	5.17	0.06	2.50	0.05	-21.443	0.954	H
IC 4051	258.7	1.42	0.06	5.34	0.07	2.75	0.05	-20.204	0.933	H
NGC 4860	280.5	1.39	0.06	5.39	0.07	2.85	0.05	-20.948	0.973	H
NGC 4923	186.0	1.70	0.05	4.43	0.05	2.69	0.04	-19.983	0.888	H
NGC 4840	216.6	1.63	0.07	4.94	0.07	2.91	0.06	-20.131	0.954	H
NGC 4869	188.1	1.40	0.05	4.83	0.05	2.90	0.04	-20.797	0.934	H
NGC 4908	192.4	1.58	0.09	4.58	0.09	2.65	0.07	-21.075	0.936	H
IC 4045	167.3	1.46	0.06	4.70	0.07	2.77	0.05	-20.282	0.943	H
NGC 4850	155.8	1.57	0.06	4.39	0.06	2.58	0.05	-19.601	0.956	H
NGC 4872	171.7	2.05	0.05	4.05	0.06	2.82	0.04	-20.893	0.874	H
NGC 4957	208.4	1.76	0.03	4.53	0.03	2.93	0.02	-21.177	0.925	H
NGC 4952	252.6	1.71	0.03	4.76	0.03	2.69	0.02	-21.203		H
GMP 1990	208.9	1.40	0.04	4.78	0.04	2.50	0.03			H
NGC 4827	243.7	1.53	0.03	4.89	0.03	2.80	0.02	-21.495	0.904	H
NGC 4807	178.5	1.81	0.06	4.39	0.06	2.78	0.05	-20.703	0.919	H
ESO 185-54	277.2	1.57	0.06	5.11	0.05	3.07	0.03	-21.861		H
NGC 3224	155.8	2.31	0.14	3.91	0.12	2.92	0.08	-20.508	0.828	H

detail, we obtain the best-fitting age and metallicity of each galaxy by minimizing the function:

$$\chi^2(t_i, Z_i) = (H\beta_i - H\beta_o)^2 + ([MgFe]_i - [MgFe]_o)^2, \quad (1)$$

where $H\beta_i$ and $[MgFe]_i$ are the $H\beta$ and $[MgFe]$ indices corresponding to the i th pair of stellar age and metallicity in the BSP model, while $H\beta_o$ and $[MgFe]_o$ are two observational indices. Moreover, we calculate the associated uncertainties of the best-fitting stellar age and metallicity for each galaxy by searching best-fitting (t, Z) s for $[H\beta_o]$ -error, $[MgFe]_o$, $[H\beta_o]$ +error, $[MgFe]_o$, $[H\beta_o]$, $[MgFe]_o$ -error and $[H\beta_o]$, $[MgFe]_o$ +error respectively and then taking their deviations from the best-fitting (t, Z) derived from $[H\beta_o]$, $[MgFe]_o$. Although the four pairs (t, Z) derived by searching do not describe perfectly well the total range of possible age and metallicity values inside the 1σ error ellipse, the maximum deviations of stellar age and metallicity can provide us with a sufficient sampling of the uncertainties involved when transposing errors from the $H\beta$ - $[MgFe]$ plane to ages or metallicities (Denicoló et al. 2005). Therefore, in this work, we take the maximum deviation as the associated 1σ uncertainty for stellar age and metallicity. Here we show the stellar ages, metallicities and their 1σ uncertainties of the main sample galaxies in Table 2. The stellar ages of these ellipticals are within the range from 3.9 to older than 15 Gyr and the stellar metallicities span over the range of 0.02 to richer than 0.03. It seems that these ages do not vary as widely as Trager et al. (2000a) whose result is 1.5 – 18 Gyr. This should result from the different stellar population synthesis model adopted in this paper. It is found

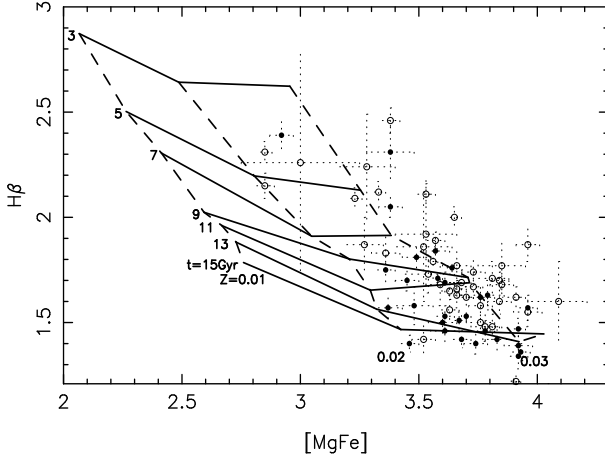


Fig. 1 Line-strength indices of our sample elliptical galaxies in the BSP model in the central $r_e/10$ aperture. Solid lines represent constant age (isochrones) and dashed lines constant metallicity (isofers). Open and filled circles represent low- and high-density ellipticals, respectively. Error bars show the observational uncertainties of two indices.

that about 78% elliptical galaxies have stellar populations older than 8 Gyr. The average stellar age of elliptical galaxies is 10.37 Gyr while the average of metallicity is 0.0277. The average 1σ uncertainties of them are 1.58 Gyr and 0.0015, respectively.

4 THE TEST OF NEW HIERARCHICAL MODEL

The hierarchical formation of elliptical galaxies has been simulated by many techniques, for example the N-body simulation and semi-analytic simulation techniques. Different models were usually carried out in the framework of a cosmological model with critical matter density and gave different predictions of stellar properties. By now, the cosmology used before has been replaced by the Λ CDM scenario. In this background, De Lucia et al. (2006) constructed a new hierarchical formation model of elliptical galaxies based on the Λ CDM scenario cosmology and studied how the star formation histories, ages and metallicities of elliptical galaxies depend on environment and on stellar mass. As a result, some special predictions are presented by this model. Firstly, it predicted that the populations of ellipticals in high-density environment would be older, more metal rich and redder than those of field ellipticals. Secondly, it predicted that the most massive elliptical galaxies would have the oldest and most metal rich stellar populations. Thirdly, it predicted that the stellar age, metallicity and galaxy color would increase with increasing stellar mass. Fourthly, the stellar mass, ages, metallicities and colors of cluster elliptical galaxies were predicted to decrease on average with increasing distance from the cluster center. In addition, the model quantified the effective progenitors of ellipticals as a function of present stellar mass and then predicted the “down-sizing” or “anti-hierarchical” of star formation histories of ellipticals in a Λ CDM universe. It is an important result, because if this model is right, we will understand the formation of elliptical galaxies much better. Therefore, it is very necessary to test this model. Of course, taking the binary interaction into the test is important because more than half of stars are binaries as we know. The detailed tests are as follows.

Table 2 Stellar ages, metallicities and associated 1σ uncertainties of 71 sample elliptical galaxies. The stellar ages and their uncertainties are in Gyr.

Name	Age	Z	Name	Age	Z
NGC 0221	4.3 ± 0.3	0.0230 ± 0.0008	NGC 2434	8.3 ± 5.9	0.0234 ± 0.0041
NGC 0315	9.0 ± 2.1	≥ 0.03	NGC 2986	12.6 ± 2.0	0.0284 ± 0.0011
NGC 0507	9.2 ± 2.3	0.0268 ± 0.0023	NGC 3078	13.9 ± 0.5	≥ 0.03
NGC 0547	11.8 ± 2.7	0.0286 ± 0.0025	NGC 3923	9.0 ± 2.5	≥ 0.03
NGC 0636	7.8 ± 0.2	≥ 0.03	NGC 5791	$\geq 15 \pm 3.2$	≥ 0.03
NGC 0720	11.2 ± 2.2	≥ 0.03	NGC 5903	10.3 ± 4.1	0.0276 ± 0.0040
NGC 0821	11.2 ± 1.7	0.0280 ± 0.0012	NGC 4261	13.0 ± 0.3	$\geq 0.03 \pm 0.0004$
NGC 1453	11.7 ± 0.3	$\geq 0.03 \pm 0.0006$	NGC 4374	13.3 ± 0.6	0.0256 ± 0.0004
NGC 1600	14.0 ± 2.0	0.0286 ± 0.0014	NGC 4472	11.4 ± 2.6	0.0296 ± 0.0032
NGC 1700	6.0 ± 0.1	≥ 0.03	NGC 4478	7.9 ± 0.7	$\geq 0.03 \pm 0.0017$
NGC 2300	11.4 ± 0.2	≥ 0.03	NGC 4489	3.9 ± 0.3	0.0254 ± 0.0012
NGC 2778	8.6 ± 1.0	$\geq 0.03 \pm 0.0010$	NGC 4552	14.3 ± 1.8	0.0285 ± 0.0014
NGC 3377	5.4 ± 0.4	0.0283 ± 0.0011	NGC 4697	9.3 ± 1.1	0.0229 ± 0.0014
NGC 3379	11.5 ± 2.7	0.0281 ± 0.0027	NGC 7562	9.7 ± 1.7	0.0283 ± 0.0017
NGC 3608	9.6 ± 1.8	0.0298 ± 0.0017	NGC 7619	13.0 ± 0.4	$\geq 0.03 \pm 0.0003$
NGC 3818	11.2 ± 2.2	≥ 0.03	NGC 7626	13.2 ± 0.8	0.0274 ± 0.0007
NGC 4278	12.3 ± 2.2	0.0258 ± 0.0023	NGC 4839	≥ 15.0	0.0242 ± 0.0007
NGC 5638	11.3 ± 1.6	0.0272 ± 0.0015	NGC 4841A	12.6 ± 2.3	0.0252 ± 0.0020
NGC 5812	11.3 ± 0.2	≥ 0.03	NGC 4926	12.9 ± 2.1	0.0246 ± 0.0018
NGC 5813	$\geq 15 \pm 0.1$	0.0217 ± 0.0009	IC 4051	13.0 ± 0.6	0.0285 ± 0.0009
NGC 5831	8.0 ± 0.2	≥ 0.03	NGC 4860	13.0 ± 2.0	$\geq 0.03 \pm 0.0018$
NGC 6127	13.5 ± 1.1	0.0268 ± 0.0019	NGC 4923	9.8 ± 4.0	0.0247 ± 0.0031
NGC 6702	4.0 ± 0.0	≥ 0.03	NGC 4840	11.4 ± 0.5	$\geq 0.03 \pm 0.0012$
NGC 7052	12.7 ± 2.0	0.0278 ± 0.0010	NGC 4869	13.0 ± 2.0	0.0272 ± 0.0027
NGC 7454	5.3 ± 0.8	0.0200 ± 0.0021	NGC 4908	12.4 ± 2.5	0.0234 ± 0.0022
NGC 7785	11.4 ± 2.6	0.0276 ± 0.0031	IC 4045	$\geq 15 \pm 0.3$	0.0230 ± 0.0010
ESO 107-04	4.6 ± 1.6	$\geq 0.03 \pm 0.0022$	NGC 4850	12.8 ± 2.1	0.0210 ± 0.0016
ESO 148-17	4.5 ± 8.6	0.0255 ± 0.0109	NGC 4872	5.8 ± 0.2	≥ 0.03
IC 4797	7.6 ± 6.3	$\geq 0.03 \pm 0.0067$	NGC 4957	8.6 ± 0.3	0.0297 ± 0.0007
NGC 0312	8.5 ± 1.6	0.0246 ± 0.0048	NGC 4952	9.4 ± 1.1	0.0275 ± 0.0005
NGC 0596	5.3 ± 0.2	≥ 0.03	GMP 1990	≥ 15.0	0.0206 ± 0.0006
NGC 0636	7.7 ± 4.4	0.0299 ± 0.0056	NGC 4827	12.4 ± 1.2	0.0268 ± 0.0012
NGC 1052	13.0 ± 0.0	≥ 0.03	NGC 4807	8.4 ± 0.8	0.0274 ± 0.0023
NGC 1395	11.8 ± 0.2	≥ 0.03	ESO 185-54	12.0 ± 2.0	$\geq 0.03 \pm 0.0012$
NGC 1407	11.1 ± 2.1	$\geq 0.03 \pm 0.0015$	NGC 3224	4.4 ± 0.9	≥ 0.03
NGC 1549	8.5 ± 0.4	0.0283 ± 0.0010			

4.1 Stellar age, metallicity and galaxy color variation with environments

A basic prediction of hierarchical galaxy formation picture is that stellar populations of more massive galaxies are older than those of less massive galaxies on average (e.g. Kauffmann 1996). This is also predicted by the model of De Lucia et al. (2006). Furthermore, De Lucia et al.'s model predicted that galaxies in denser environment would have more metal rich and redder populations than ellipticals. These specialties are thought to be attributed to the fact that high density regions form from the highest density peaks in the primordial field of density fluctuations. Here we test these specialties with our data.

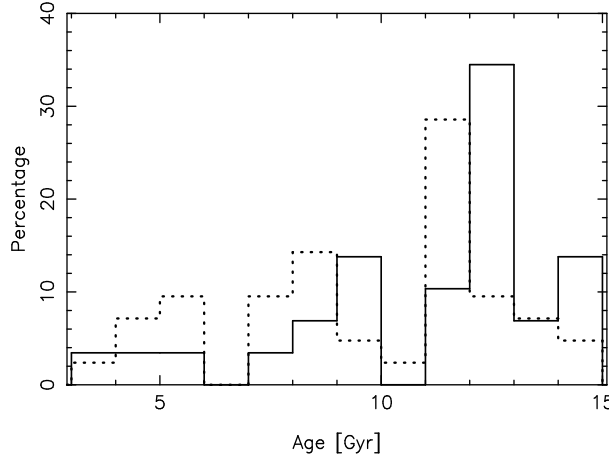
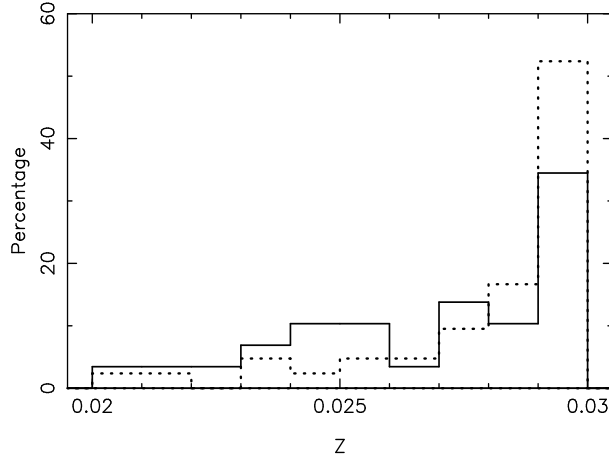


Fig. 2 Stellar age distribution of low- and high-density elliptical galaxies. The dashed and solid lines show the distribution of low- and high-density ellipticals, respectively.



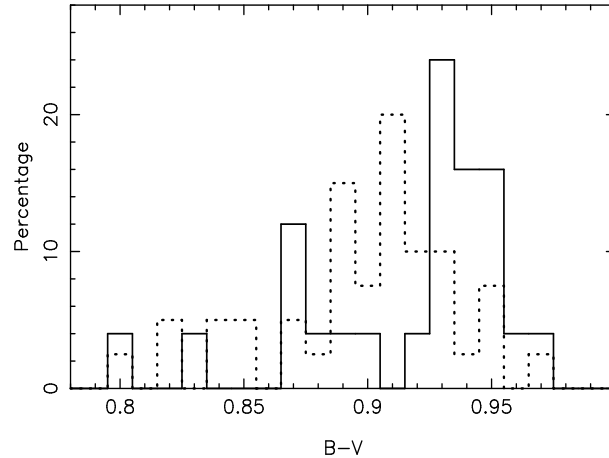


Fig. 4 $B - V$ distribution of low- and high-density elliptical galaxies. The dashed and solid lines have the same meanings as in Fig. 2.

metal rich than those of low-density ellipticals. We also can see this trend clearly from Fig. 1 that ellipticals in high-density environment really distribute in the lower metallicity region than those field ellipticals. In the figure, filled circles represent ellipticals in high-density environment.

When we study the $B - V$ color distribution of two type elliptical galaxies, the result is consistent with De Lucia (2006) model (see Fig. 4 in more detail). On average, ellipticals in high-density environment are about 0.02 mag redder than those in low-density environment.

4.2 Stellar age, metallicity and galaxy color variation with stellar mass

The most important result and prediction of the De Lucia model is that the most massive elliptical galaxies have the oldest and most metal rich stellar populations. Besides, the model predicted that the stellar age, metallicity and galaxy color would increase with increasing stellar mass. We test these predictions in Figs 5, 6 and 7, respectively. Here the stellar masses of elliptical galaxies are calculated by the fitting function suggested by Thomas et al. (2005):

$$\log(M_*/M_\odot) = 0.63 + 4.52\log(\sigma_0/(\text{km s}^{-1})), \quad (2)$$

where M_* is the stellar mass and σ_0 is the velocity dispersion. According to previous studies, there is usually a relation between the mass and luminosity of elliptical galaxies, e.g. $(M/L)_B = (5.93 \pm 0.25)h_{50}$ (van der Marel 1991). It means that the luminous elliptical galaxies have the massive masses. Therefore the absolute magnitude is usually used for a indicator of stellar mass of galaxies (e.g. Terlevich & A. Forbes D. 2002). In order to study the reliability of the mass estimation presented above, we compare the stellar masses calculated by the function with absolute B-band magnitudes of these galaxies, which are taken from HyperLeda database (<http://www.brera.mi.astro.it/hypercat/>). As a result, we find that luminous elliptical galaxies have more massive stellar masses. Therefore, as a whole, the stellar masses estimated by the fitting function can express the real stellar masses of elliptical galaxies well.

In Fig. 5, stellar age is plotted as a function of stellar mass. The filled squares with error bars are look-back times and stellar masses predicted by the De Lucia model. The look-back

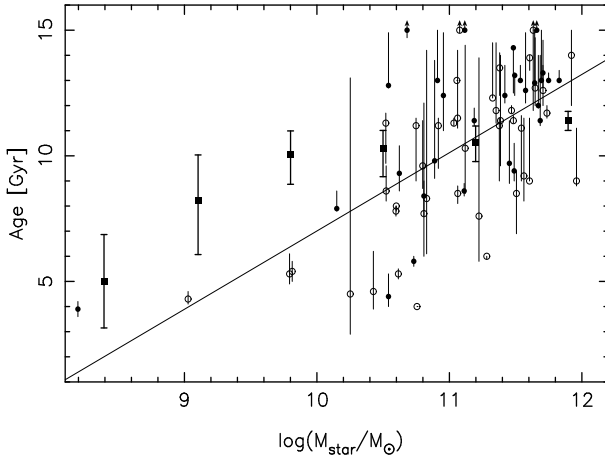


Fig. 5 Stellar age - mass relation of 71 elliptical galaxies. Filled squares with error bars are predictions of galaxy formation model. With arrows, some galaxies that have stellar populations possibly older than the maximum age of BSP model (15 Gyr) are shown. The solid line is a linear least-squares fit to the data. Open and filled circles represent low- and high-density ellipticals, respectively.

time of a galaxy is the time corresponding to the redshift when 50 percent of the stars were first formed. Open and filled circles with arrows show galaxies that have stellar ages possibly older than 15 Gyr (the maximum age of the BSP model). It is easy to see a trend that more massive ellipticals have older stellar populations and the most massive galaxies have the oldest stars. But the changing of stellar age with stellar mass is different from the model prediction. This is perhaps caused by the somewhat different definitions of look-back time and stellar age. In detail, the stellar age in the simple BSP model is defined corresponding to the redshift when all stars formed at the same time. When we fit the relation between stellar age and stellar mass, we find a linear relation: $\text{age} = 3.115 \log(M_*/M_\odot) - 24.147$, with a 0.656 correlation parameter.

In Fig. 6, we show the stellar metallicity - stellar mass relation of the main sample elliptical galaxies. The open and filled circles with arrows show ellipticals that have populations possibly more metal rich than 0.03 (the maximum metallicity of the BSP model). The open pentacles with dashed error bars represent the predictions of De Lucia model. From this plot, we see that all galaxies have metallicities richer than the predictions of De Lucia model. However, if we only take ellipticals with stellar metallicities lower than 0.03 into account, our data can be expressed by a trend similar to the prediction of De Lucia model, which can be derived by adding 0.074 (the difference between the maximum metallicity of De Lucia model and that of the BSP model) to each stellar metallicity predicted by De Lucia model. We plot the trend via filled pentacles with solid error bars, which can be seen clearly in Fig. 7. It means that our data have the same trend as the prediction of De Lucia model. In fact, the result is possibly limited by the theoretical models, thus the difference between our data and prediction of the galaxy formation model is understandable.

The relation between galaxy color and stellar mass is plotted in Fig. 7. The stellar masses are calculated by this work using eq. (2). Filled circles in the plot represent ellipticals in high-density environment and open circles represent the field ellipticals. Filled squares with error

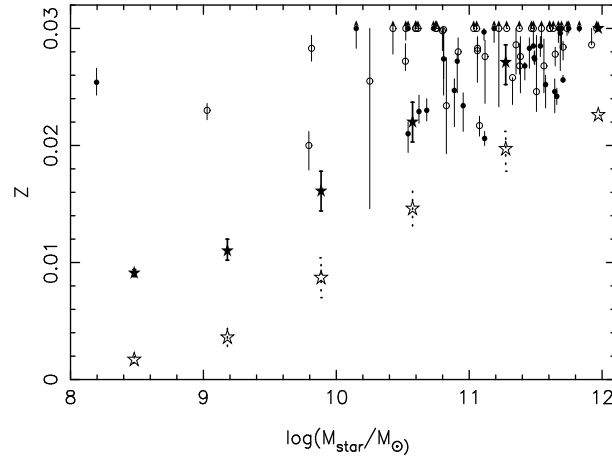


Fig. 6 Stellar metallicity – mass relation of our sample elliptical galaxies. Galaxies that have stellar metallicities larger than the maximum metallicity available for BSP model (0.03) are shown with arrows. The open pentacles with dashed error bars represent the predictions of De Lucia model and the filled pentacles with solid error bars represent the metallicities of De Lucia model added by 0.074. The open and filled circles have the same meanings as in Fig. 5.

bars represent the color versus stellar mass relation predicted by the model. We see that our data agree with the relation predicted by the model very well.

4.3 Stellar age, metallicity, mass and color variation with cluster-centric distance

The De Lucia model predicted a clear trend driven by mass segregation and incomplete mixing of the galaxy population during the cluster assembly. According to the prediction, within clusters, stellar masses, ages, metal abundances and galaxy colors would decrease on average with increasing distance from the cluster center. To test these trends, we select 11 component elliptical galaxies of Fornax cluster and determine their stellar ages and metallicities from $H\beta$ and $[Mg/Fe]$ line indices within $r_e/8$. The line indices of these galaxies are derived from Kuntschner (2000) and their coordinates and $B-V$ colors are derived from HyperLeda database (<http://www.brera.mi.astro.it/hypercat/>). Here we show the main data of 11 ellipticals in Table 3. It is noticeable that we use the angular distance to the centric galaxy NGC 1399 (a galaxy well studied, e.g. Loewenstein et al. 2005) instead of the real cluster-centric distance for each elliptical galaxy, because it is difficult to determine the accurate distances of galaxies while they have uncertain peculiar velocities. The main results are shown in Figs 8, 9 and 10.

In Fig. 8, stellar metallicity is plotted as a function of angular distance to NGC1399 (θ_{1399}). We see that it is difficult to find a clear trend in the whole angular distance range. But within a small range, e.g. 2.5 arcmin, the stellar metallicity seems to decrease with increasing angular distance.

The relation of $B-V$ color and angular distance is shown in Fig. 9 while the relation of stellar mass and angular distance in Fig. 10. The two plots do not show clear support or

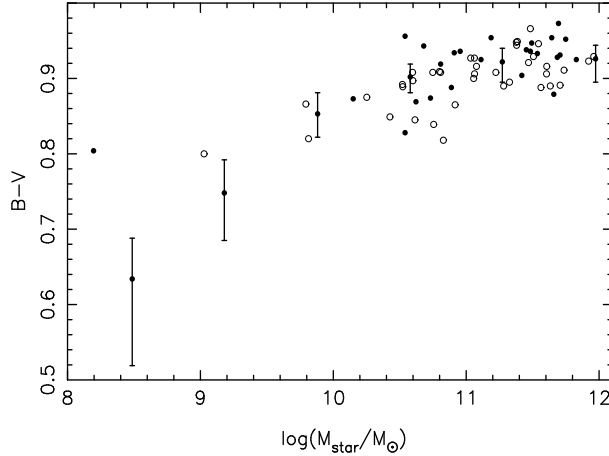


Fig. 7 $B - V$ and stellar mass relation of the sample elliptical galaxies. The stellar masses are calculated by this work. Filled squares with error bars represent the values predicted by the model. Open and filled circles have the same meanings as in Fig. 5.

Table 3 Main data for 11 component elliptical galaxies of the Fornax cluster. In the table, $\log M_*$ is the logarithm of stellar mass and θ_{1399} is the angular distance to NGC 1399.

Name	$\log(M_*/M_\odot)$	θ_{1399} [arcmin]	$B - V$ [mag]	Age [Gyr]	Z [Gyr]
NGC 1336	9.5886	0.324	0.809	14.6 ± 4.9	0.0179 ± 0.0029
NGC 1339	10.5695	3.318	0.903	13.8 ± 2.4	0.0270 ± 0.0030
NGC 1351	10.5559	0.636	0.844	14.8 ± 2.9	0.0235 ± 0.0039
NGC 1373	9.1050	0.294	0.832	8.6 ± 1.9	0.0212 ± 0.0038
NGC 1374	10.8768	0.240	0.894	11.8 ± 2.3	0.0299 ± 0.0041
NGC 1379	10.1853	0.036	0.866	9.8 ± 4.7	0.0241 ± 0.0039
NGC 1399	12.2645	0	0.934	14.1 ± 0.9	≥ 0.03
NGC 1404	11.5458	0.150	0.941	$\geq 15 \pm 3.0$	≥ 0.03
NGC 1419	9.9774	2.160	0.863	14.9 ± 2.8	0.0159 ± 0.0034
NGC 1427	10.7684	0.084	0.885	11.1 ± 3.0	0.0262 ± 0.0034
IC 2006	10.2757	0.588	0.896	13.7 ± 1.0	0.0294 ± 0.0010

opposition to the model, neither. In addition, it is found that the trend between stellar age and mass, which we do not show here, seems almost random.

In Figs 8, 9 and 10, we see that there are only 3 galaxies with angular distance farther than 0.6 arcmin, we suggest the less elliptical galaxies that farther than 0.6 arcmin must affect all trends relating to cluster-centric distance. Furthermore, the small sample of elliptical galaxies we used perhaps affects the results.

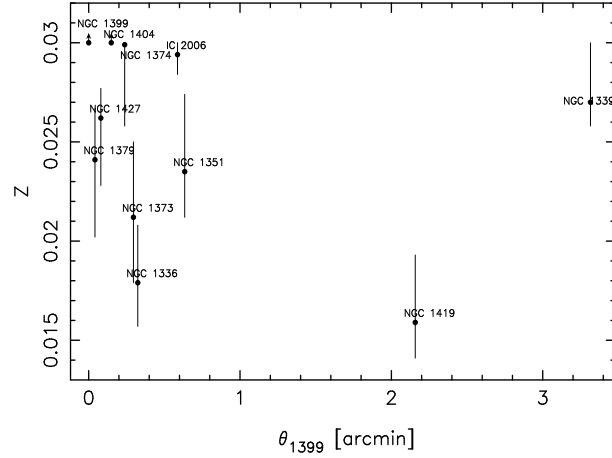


Fig. 8 The plot of elliptical galaxies in (Z, θ_{1399}) plane. Z and θ_{1399} are stellar metallicity and angular distance to NGC 1399, respectively.

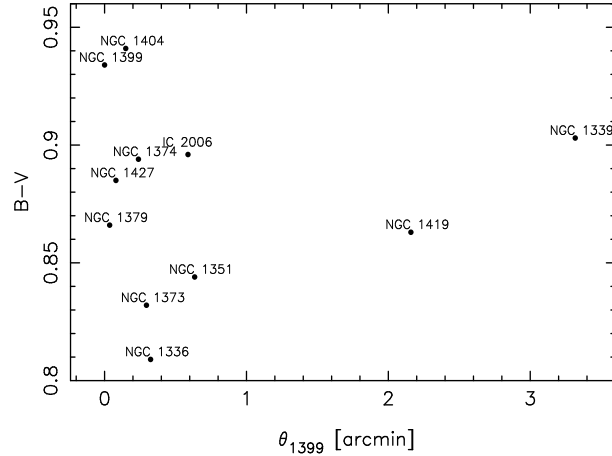


Fig. 9 The plot of elliptical galaxies in $(B - V, \theta_{1399})$ plane. θ_{1399} has the same meaning as in Fig. 8.

5 DISCUSSION AND CONCLUSION

We determined stellar ages and metallicities of about 80 elliptical galaxies using the BSP model of Zhang et al. (2005b) and test the latest formation model of elliptical galaxies (De Lucia 2006) for the first time. We find that elliptical galaxies have stellar populations about 10 Gyr old and more metal rich than 0.02 (see also Zhou et al. 1992).

When we analysis our data, we find that stellar populations of elliptical galaxies in high-density environment are about 1.5 Gyr older while 0.001 less metal rich than those of field

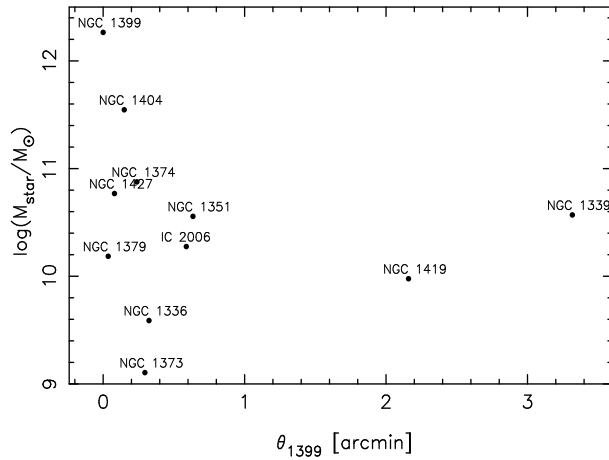


Fig. 10 The plot of elliptical galaxies in $[\log(M_{\text{star}}/M_{\odot}), \theta_{1399}]$ plane. $\log(M_{\text{star}}/M_{\odot})$ represents stellar mass of galaxies and θ_{1399} has the same meaning as in Fig. 8.

elliptical galaxies. We also find that elliptical galaxies in high-density environment are about 0.02 mag redder than field ellipticals. Furthermore, we find that more massive ellipticals are redder and have older and more metal rich stellar populations than those less massive ones. It also seems that the most massive ellipticals have the oldest and most metal rich populations. However, elliptical galaxies in low-density environment show more metal rich stellar populations than those high-density complements. In fact, this trend is completely opposite to the prediction of De Lucia et al. model. When we test the stellar mass, age, metallicity and galaxy color variation with the cluster-centric distance, the results do not show clear support or opposition to the model and it seems that they are affected by using the angular distance instead of cluster-centric distance and the small elliptical galaxy sample we used. Therefore, the results derived from BSP model support the Λ CDM-based hierarchical model of elliptical galaxies formation, expect the metallicity distribution with environments and the changing of stellar peculiarities with cluster-centric distance. However, the doubtless conflict between our result and prediction of the model, i.e. the result that low-density elliptical galaxies have more metal rich populations than high-density elliptical galaxies, should be paid attention to.

Acknowledgements We thank HyperLeda team for supplying us with the photometry of galaxies on the internet: <http://www.brera.mi.astro.it/hypercat/>. We also thank Prof. Xu Zhou and Prof. Tinggui Wang for some useful discussions. This work is supported by the Chinese National Science Foundation (Grant Nos 10433030, 10521001 and 10303006), the Chinese Academy of Science (No. KJX2-SW-T06) and Yunnan Natural Science Foundation (Grant No. 2005A0035Q).

References

Barger A. J., Aragon-Salamanca A., Ellis R. S., Couch W. J., Smail I., Sharples R. M., 1996, MNRAS, 279, 1
 Baugh C. M., Cole S., Frenk C. S., Lacey C. G., 1998, ApJ, 498, 504
 Baugh C. M., Cole S., Frenk C. S., 1996, MNRAS, 283, 1361
 Beuing J., Bender R., Mendes de Oliveira C., Thomas D., Maraston C., 2002, A&A, 395, 431

Bruzual G., Charlot S., 2003, MNRAS, 344, 1000

Cole S., Lacey C. G., Baugh C. M., Frenk C. S., 2000, MNRAS, 319, 168

De Lucia C., Springel V., White S. D. M., Croton D., 2006, MNRAS, 366, 499

Denicoló G., Terlevich R., Terlevich E., Forbes D. A., Terlevich A., 2005, MNRAS, 358, 813

González J., 1993, Ph.D. thesis, Univ. California, Santa Cruz

Kauffmann G., White S. D. M., Guiderdoni B., 1993, MNRAS, 264, 201

Kauffmann G., 1996, MNRAS, 281, 487

Kauffmann G., Charlot S., 1998, MNRAS, 294, 705

Kodama T., Arimoto N., Barger A. J., Aragón-Salamanca A., 1998, A&A, 334, 99

Kormendy J., 1987, In: S. M. Faber, ed., *Nearly Normal Galaxies: From the Planck Time to the Present*, New York: Springer-Verlag, 81

Kormendy J., Djorgovski S., 1989, ARA&A, 27, 235

Kuntschner H., 2000, MNRAS, 315, 184

Lauberts A., Valentijn E. A., 1989, The Surface Photometry Catalogue of the ESO-Uppsala Galaxies, Garching: ESO

Loewenstein M., Angelini L., Mushotzky R. F., 2005, ChJAA, 5, 335

Mehlert D., Saglia R. P., Bender R., Wegner G., 2000, A&AS, 141, 449

Mehlert D., Thomas D., Saglia R. P., Bender R., Wegner G., 2003, A&A, 407, 423

Peebles P. J. E., 1980, *The Large-Scale Structure of the Universe*, Princeton: Princeton University Press

Terlevich A. I., Forbes D., 2002, MNRAS, 330, 547

Thomas D., 1999, MNRAS, 306, 655

Thomas D., Maraston C., Bender R., de Oliveira, Claudia M., 2005, ApJ, 621, 673

Thomsen B., Baum W. A., 1989, ApJ, 347, 214

Toomre A., Toomre J., 1972, ApJ, 178, 623

Trager S. C., Faber S. M., Worthey G., González J. J., 2000a, AJ, 119, 1645

Trager S. C., Faber S. M., Worthey G., González J. J., 2000b, AJ, 120, 165

van der Marel R. P., 1991, MNRAS, 253, 710

van Dokkum P. G., Stanford S. A., 2003, ApJ, 585, 78

van Zee L., Barton E. J., Skillman E. D., 2004, AJ, 128, 2797

Vazdekis A., 1999, ApJ, 513, 224

Vazdekis A., Casuso E., Peletier R. F., Beckman J. E., 1996, ApJS, 106, 307

Vazdekis A., Peletier R. F., Beckman J. E., Casuso E., 1997, ApJS, 111, 203

Worthey G., 1994, ApJS, 95, 107

Zhang F. H., Han Z. W., Li L. F., Hurley J. R., 2005a, MNRAS, 357, 1088

Zhang F. H., Li L. F., Han Z. W., 2005b, MNRAS, 364, 503

Zhou X., Véron-Cetty M.-P., Véron P., 1992, ACTA ASTROPHYSICA SINICA, 12, 308